

***N*-linked glycan sites on the influenza NA head domain are required for efficient IAV incorporation and replication**

Henrik Östbye¹, Jin Gao², Mira Rakic Martinez², Hao Wang¹, Jan-Willem de Gier¹ and Robert Daniels^{2*}

¹*Department of Biochemistry and Biophysics, Stockholm University, 10691 Stockholm, Sweden.* ²*Division of Viral Products, Center for Biologics Evaluation and Research, Food and Drug Administration, Silver Spring, MD 20993, USA*

*Correspondence: Robert.Daniels@fda.hhs.gov

Running Title: *Analysis of N-linked glycan sites in the NA head domain*

ABSTRACT

N-linked glycans commonly contribute to secretory protein folding, sorting and signaling. For enveloped viruses such as the influenza A virus (IAV), the addition of large *N*-linked glycans can also prevent access to epitopes on the surface antigens hemagglutinin (HA or H) and neuraminidase (NA or N). Sequence analysis showed that in the NA head domain of H1N1 IAVs three *N*-linked glycosylation sites are conserved and that a fourth site is conserved in H3N2 IAVs. Variable sites are almost exclusive to H1N1 IAVs of human origin, where the number of head glycosylation sites first increased and then decreased over time. In contrast, variable sites exist in H3N2 IAVs of human and swine origin, where the number of head glycosylation sites has mainly increased over time. Analysis of IAVs carrying N1 and N2 mutants demonstrated that the *N*-linked glycosylation sites on the NA head domain are required for efficient virion incorporation and replication in cells or eggs. It also revealed that N1 stability is more affected by the head domain glycans, suggesting N2 is more amenable to glycan additions. Together, these results indicate that in addition to antigenicity, *N*-linked glycosylation sites can alter NA enzymatic stability and the NA amount in virions.

Key words: Influenza neuraminidase, *N*-linked glycosylation sites, IAV composition, stability, glycoprotein maturation.

39 INTRODUCTION

40 Glycoproteins receive *N*-linked glycans when they are inserted into the endoplasmic
41 reticulum (ER) lumen. Addition of these large oligosaccharide structures can lower the
42 activation barrier for the glycoprotein to fold and can function as docking sites for cellular
43 factors that assist in the folding, quality control and the trafficking of the newly synthesized
44 glycoprotein [1-4]. Following the maturation process, *N*-linked glycans can also contribute to
45 the function of the glycoprotein by influencing local conformations, extending the half-life, or
46 directly participating in critical protein interactions [5-9]. Many envelope viral glycoproteins
47 utilize *N*-linked glycans for these common cellular functions [10-12], and for the ability of the
48 large glycan structures to limit access to sensitive epitopes [13-17]. For influenza viruses, the
49 roles of *N*-linked glycans in the folding and masking of epitopes on its surface glycoprotein
50 hemagglutinin (HA or H) have been well-established [13, 18-20]. However, a comprehensive
51 picture is lacking for how *N*-linked glycans contribute to the other influenza glycoprotein
52 neuraminidase (NA or N), as only a few experimental studies have been performed [17, 21].

53 The HA and NA glycoproteins from influenza A viruses (IAVs) are quite diverse and
54 are classified into subtypes based on their antigenic and genetic properties [22]. Presently,
55 sixteen HA (designated H1-H16) and nine NA (designated N1-N9) subtypes have been
56 identified in avian IAVs in almost every possible combination [23]. Despite this variability,
57 only H1N1 and H3N2 subtypes seasonally circulate in the human population, and they are also
58 commonly isolated from swine species, which are susceptible to both avian and human IAVs
59 [24, 25].

60 There are some similarities between the numerous NA subtypes. All are type II
61 membrane glycoproteins that form a Ca²⁺-dependent tetrameric enzyme [26-30]. The enzymatic
62 function, located in the C-terminal head domain, promotes the mobility of the virus by
63 removing the terminal sialic acid residues that HA binds to on host and viral glycan structures
64 [31, 32]. During IAV replication, NA is co-translationally targeted to the ER by its *N*-terminal
65 transmembrane domain of varying hydrophobicity [27, 33, 34]. The transmembrane domain
66 then inverts and integrates into the ER membrane as the C-terminal stalk and head domain are
67 synthesized and translocated into the ER lumen [34]. Upon entering the Ca²⁺-rich ER lumen
68 the stalk and the enzymatic head domain receive multiple *N*-linked glycans that are capable of
69 recruiting chaperones [21, 35]. The chaperones likely assist in the folding and oligomerization
70 of NA, which occurs through a cooperative process that involves the enzymatic head and the
71 distal transmembrane domain [21, 36-38].

72 Previous work focused on the *N*-linked glycans of NA showed that an avian N9 variant
73 predominantly misfolds in CHO cells when not glycosylated and that the misfolding is mainly
74 caused by the loss of the head domain glycans [21]. More recent studies on H1N1 IAVs have
75 begun to examine the temporal frequency of *N*-linked glycosylation sites in N1[39-41], and the
76 heterogeneity of the *N*-linked glycan structures[35]. The positional analysis has led to the
77 speculation that many N1 glycan sites correlate with antigenic regions[40], whereas the glycan
78 analysis identified a single site on the N1 head domain that is modified by a wide variety of
79 glycans, with a diverse antenna array when expressed in eggs[35]. However, the impact of these
80 sites on NA has not been looked at directly for H1N1 IAVs and even less data is available for
81 these sites from H3N2 IAVs.

82 Here, we examined the glycosylation site frequencies in the NA sequences from H1N1
83 and H3N2 strains by domain (stalk versus head), year of isolation and species of origin. Three
84 conserved sites were identified in the N1 head domain and four in the N2 head domain. For the
85 N1 head domain, variable glycosylation sites are almost exclusive to human H1N1 IAVs,
86 whereas the N2 head domain has more variable sites and these are present in human, swine and
87 avian H3N2 IAVs. Analysis of viruses carrying NAs with mutated glycosylation sites revealed
88 that the ones in the head domain are required for efficient virion incorporation and replication,
89 and influence NA stability in a subtype-dependent manner. These results illustrate how *N*-
90 linked glycans on NA can perform multiple functions and may explain why variable
91 glycosylation sites are more prevalent in N2.

92
93

94 **RESULTS**

95 *Analysis of the N-linked glycan sites encoded by the NA from H1N1 IAVs*

96 *N*-linked glycans are transferred to the Asn in the consensus sequence N-X-S/T-X, where X
97 can be any amino acid other than Pro [42, 43]. The addition of the glycan occurs on the luminal
98 side of the ER membrane (Fig. 1A), limiting the accessibility of some regions in membrane
99 proteins. Influenza NA is synthesized as a type II membrane glycoprotein with the N-terminus
100 in the cytosol and a long C-terminal region in the ER lumen (Fig. 1B). The C-terminal region
101 contains the stalk and head domain, and both of these regions have been shown to encode
102 multiple *N*-linked glycosylation sites [21, 34, 39-41]. To determine if the glycosylation sites in
103 NA have a domain or temporal bias with respect to the IAV species of origin, we initially
104 examined the available subtype 1 (N1) sequences from H1N1 IAVs. The sequence analysis
105 showed that the majority (~92%) of avian N1s possess seven predicted *N*-linked glycan sites,

106 whereas the human and swine N1s tend to have more sites and vary in the site number (Fig. 1C,
107 left panel). In the stalk, most avian N1s have four sites and the human and swine N1s mainly
108 carry four or five (Fig. 1C, middle panel). In the head domain, avian N1s predominantly have
109 three sites, whereas the swine N1s contain either three or four, and the human N1s range from
110 three to five (Fig. 1C, right panel). In line with previous reports [39, 41], these differences
111 indicate that the stalk and head domain both contribute to the species-related variation in the
112 number of NA glycosylation sites, but it remains unclear if the bias relates to how the sequences
113 were collected.

114
115 Some glycosylation sites in the NA head have been linked to antigenicity [17], therefore we
116 performed a temporal analysis of the sites in the N1 head domain. Regardless of the year the
117 strain was isolated, the avian N1 head domains were found to mainly contain three sites (Fig.
118 1D, left panel) and the swine N1 head domains fluctuated between three to four sites with no
119 temporal pattern (Fig. 1D, middle panel). In contrast, the human N1 head domains showed a
120 step-wise pattern, with the early strains increasing in the number of sites from three to six, and
121 the more recent strains decreasing back to three (Fig. 1D, right panel). These temporal
122 observations indicate that the addition and removal of *N*-linked glycan sites in the N1 head
123 domain is more characteristic of human H1N1 IAVs and that N1 likely requires at least three
124 glycosylation sites in the head domain.

125
126 *Location of the N-linked glycan sites in the NA head domain of H1N1 IAVs*

127 Positional analysis revealed that three *N*-linked glycosylation sites are highly conserved in the
128 N1 head domain in H1N1 IAVs (Fig. 2A). *In silico* modelling of minimal glycan structures
129 onto these sites showed that one (Asn146) is positioned on the top of the NA tetramer and the
130 other two (Asn88 and Asn235) are located close together on the bottom, facing the viral
131 membrane (Fig. 2B). One of the four prevalent variable sites in the human N1 head domain
132 (Asn386) is also frequently found in the swine N1 head domain (Fig. 2C), likely due to the
133 swine origin of the human 2009 pandemic H1N1 virus. Temporally, the prevalent variable sites
134 overlap for different time periods, contributing to the discrete changes observed in the number
135 of glycosylation sites on the human N1 head domain (Fig. 2C and 1F). Positionally, three of
136 the variable sites (Asn365, Asn386, and Asn455) cluster towards the NA tetramer side (Fig.
137 2D), which has previously been shown to be an antigenic region in NA [44]. The final prevalent
138 variable site at Asn434 is located very close to the conserved site at Asn146 (Fig. 2D),

139 suggesting these two sites, and possibly the other two conserved sites (Asn88 and Asn235),
140 perform redundant roles.

141

142 *The conserved N1 head glycosylation sites are not essential for viral replication in cells*

143 Although the glycosylation sites at Asn88, Asn146 and Asn235 are highly conserved in the N1
144 head domain (Fig. 3A), we were able to identify sequences that carry a mutation in one of the
145 sites (S90P, T148A, and N235K). These natural mutations were then introduced into a NA (N1-
146 MI15) from a previously recommended 2009 pandemic-like H1N1 vaccine strain
147 (A/Michigan/45/2015) in various combinations to determine if the conserved sites are required
148 for H1N1 IAV replication. We chose N1-MI15 for the analysis as it does not contain any
149 variable head glycan sites. An additional mutation (S90A) was also included to alleviate
150 potential folding concerns associated with the S90P mutation that introduces a Pro residue.

151

152 Surprisingly, all the recombinant viruses carrying the N1-MI15 single, double and triple glycan
153 site mutants were rescued using a WSN33 backbone. These single-gene reassortant viruses,
154 along with a N1-MI15 wild-type (WT) control, were propagated in MDCK cells, isolated by
155 sedimentation, and analysed. Each of the N1-MI15 variants in the sedimented virions possessed
156 enzymatic activity and resolved as intermolecular disulphide bonded dimers following non-
157 reducing (NR) SDS-PAGE (Figs. 3B and 3C), which is a characteristic of properly folded N1
158 [26, 36]. The expected mobility increase was more pronounced for N1-MI15 with the triple and
159 double glycosylation site mutants than for the single site mutants (Figs. 3B and 3C), implying
160 the appropriate glycans were likely absent in the mutants. We also noted that visualization of
161 the double and triple glycan site mutants required higher volumes of the sedimented viral-
162 containing medium (Fig. 3C), suggesting the absence of several conserved glycans modestly
163 impairs viral growth by decreases NA folding or trafficking.

164

165 *The conserved glycosylation sites in the N1 head are not essential for viral replication in eggs*

166 Several factors can potentially influence the results obtained after the conserved glycan sites
167 were mutated in N1-MI15, including the use of the natural mutations, the particular NA, the
168 viral backbone and the growth environment. Therefore, we repeated the analysis with a NA
169 (N1-BR18) from a more recently recommended 2009 pandemic-like H1N1 vaccine strain
170 (A/Brisbane/02/2018) using a different mutation strategy (N to Q), backbone (PR8) and growth
171 environment (embryonated eggs). Like the prior results, all the recombinant viruses carrying
172 N1-BR18 with single, double and triple mutations in the head glycan sites were rescued. Upon

173 passaging in eggs lower hemagglutinating unit (HAU) titres were only observed for the two
174 double glycan site mutants lacking the Asn146 site and the triple glycan site mutant (Fig. 4A,
175 upper graph). Variable NA activity was measured in the egg allantoic fluid for all the viruses
176 apart from the triple glycan site mutant, which consistently produced low activity levels (Fig.
177 4A, lower graph). Each of the N1-BR18 mutants displayed increased mobility on reducing (RD)
178 and NR SDS-PAGE, which correlated with the number of the glycosylation site mutations (Fig.
179 4B), indicating the mutations remained intact. Together, these results demonstrate that the
180 conserved *N*-linked glycosylation sites on the N1 head domain are not essential for H1N1 virus
181 replication in cells or embryonated eggs. However, we did observe that viral replication appears
182 to decrease when the three conserved head glycan sites are mutated (Fig. 4A) and that N1
183 intermolecular disulphide-bond formation and virion incorporation are less efficient when two
184 glycan sites are absent (Fig. 4B).

185

186 *The conserved glycans on the head domain influence N1 viral incorporation*

187 When the three conserved glycan sites in the N1-BR18 head domain were mutated, the PR8
188 backbone virus showed a tendency in eggs to reach lower HAU titres and NA activity levels
189 (Fig. 4A). This raised several questions: is the phenotype backbone dependent; do the mutations
190 change the HA to NA ratio in the virions, or cause a decrease in viral production? To address
191 these questions, we rescued a wildtype N1-BR18 virus (WT) and a mutant containing no head
192 glycosylation sites (NHG 3Q) using a WSN backbone. Upon passaging in eggs both the HAU
193 titre and the NA activity in the allantoic fluid were significantly lower when the three conserved
194 glycosylation sites on the N1 head domain were mutated (Fig. 5A, compare WT to NHG 3Q),
195 demonstrating the phenotype is conserved and may be somewhat exacerbated with a WSN
196 backbone.

197

198 The lower HAU titres for the virus carrying the N1-BR18 mutant (NHG 3Q) indicated that the
199 conserved glycosylation sites on the N1 head domain do contribute to viral production. To
200 address if the mutations changed the HA to NA ratio in the virus, we isolated the virions by
201 centrifugation and examined equal quantities of total protein by SDS-PAGE followed by
202 Coomassie staining. In the absence of the reductant dithiothreitol (DTT), oxidized N1-BR18
203 dimers were readily apparent for the WT virus and these were reduced to the expected
204 molecular weight upon DTT addition (Fig. 5B). Despite the relatively equivalent levels of HA,
205 NP and M1, a band corresponding to N1-BR18 with the three glycan site mutations (NHG 3Q)
206 was not observed, indicating the HA to NA ratio increased (Fig. 5B). Although the N1-BR18

207 mutant was not visible by Coomassie staining, the virus displayed NA activity levels ~20% of
208 the WT when equal viral protein amounts were analysed (Fig. 5B) and the protein was also
209 detected as a less intense faster migrating band by immunoblotting (Fig. 5C). Together, these
210 results demonstrate that H1N1 viral production and NA incorporation both decrease when all
211 three conserved glycosylation sites are absent on the N1 head domain.

212

213 *The variable glycosylation sites in the N1 head domain from human H1N1 IAVs*

214 Previous studies have demonstrated that the N-linked glycosylation sequence N-X-T is more
215 efficiently recognized than N-X-S [43]. Based on sequence alignments of the human N1 head
216 domain three of the main variable glycosylation sites (Asn365, Asn386 and Asn455) use N-X-
217 S and these sites likely change by substitutions at either the N or S residues (Fig. 6A). In contrast,
218 the other variable glycosylation site (Asn434) uses N-X-T and appears to have been created by
219 a T codon insertion combined with a N substitution that occurred later (Fig. 6B). The codon
220 insertion is almost exclusively found in human H1N1 IAVs beginning in 1948 and ending when
221 the 2009 pandemic H1N1 virus, which carries a N1 gene segment of swine origin, was
222 introduced to the human population (Fig. 6B). Positionally, the Asn434 site is located near the
223 conserved Asn146 site and out of the seven most prevalent glycosylation sites, these are the
224 only two with the more efficient recognition sequence, suggesting they may impact N1 more
225 than the others.

226

227 To investigate this site, two similar natural sequences were identified that lack or have the
228 insertion resulting in the Asn434 glycosylation site. Several mutations were then introduced
229 into the NA lacking the insertion (N1-NY09), which is from a 2009 pandemic-like H1N1 strain
230 (A/New York/18/2009), and a NA possessing the insertion (N1-WA01), which is from a 2001
231 seasonal H1N1 strain (A/Waikato/7/2001). For N1-NY09 these involved creating a
232 glycosylation site by mutation (I436T), codon insertion (+435T), and a control where a codon
233 insertion (+436A) was made that does not create a glycosylation site. All the mutants were
234 rescued using a WSN backbone and propagated using MDCK cells where no growth defect was
235 observed based on cytopathic effects. Activity measurements and immunoblot analysis of the
236 isolated particles showed no significant change in the N1-NY09 levels and the mutants with the
237 additional glycosylation site (I436T and +435T) displayed the expected mobility increase (Fig.
238 6C). Similar results were obtained from viruses carrying N1-WA01 with converse mutations
239 that removed the glycosylation site (T436A), the codon insertion responsible for the
240 glycosylation site (-435T) or a downstream codon (-437I) that left the site (Fig. 6D).

241

242 As Asn434 is near the central Ca²⁺ binding site, which is a major determinant for NA stability
243 [26], we asked if this glycan influences NA thermostability. For N1-NY09, introducing the
244 insertion and the glycosylation site (+435T) caused the thermostability to drop to a level that
245 almost matched N1-WA01. Conversely, deleting this codon (-435T) in N1-WA01 increased the
246 thermostability to the level of N1-NY09 (Fig. 6E). However, the analysis of the other mutants
247 indicated that the stability changes are more associated with the insertion (*see* +436A) for N1-
248 NY09 and deletion (*see* -437I) for N1-WA01 than the glycan addition or removal (Fig. 6E).
249 This implies that structural changes imparted by the codon insertion or deletion may affect N1
250 stability by altering the oligomeric assembly that creates the central Ca²⁺ binding site. We then
251 tested this more broadly by examining the conserved head glycan site mutants. Interestingly,
252 all N1-MI15 mutants lacking the N-X-T site at Asn146 (148A) possess decreased
253 thermostability, indicating that both N-X-T head glycosylation sites contribute to N1
254 thermostability (Fig. 6F).

255

256 *Analysis of N-linked glycan sites encoded by the NA from H3N2 IAVs*

257 H3N2 IAVs commonly circulate together with H1N1 IAVs in the human population. Therefore,
258 we also analysed the subtype 2 (N2) sequences from H3N2 IAVs. In contrast to N1, the avian,
259 swine and human N2 sequences all vary in the number of predicted N-linked glycosylation sites,
260 with swine N2s having the most, followed by the human and avian N2s (Fig. 7A, left panel).
261 Surprisingly, almost all N2 sequences were found to contain two sites in the stalk (Fig. 6A,
262 middle panel), resulting in the head domain being responsible for the variation in the number
263 of N2 glycosylation sites (Fig. 7A, right panel).

264

265 Positional analysis showed that four of the N-linked glycosylation sites are highly conserved in
266 the N2s and that many variable sites showed a bias based on the species of origin of the strain
267 (Fig. 7B). Of the four conserved sites, three (Asn86, Asn146 and Asn234) are nearly identical
268 to N1 and the fourth (Asn200) is located on the side near the dimer interface. In contrast to N1,
269 N-X-T is the most prevalent glycosylation sequence in the N2 head as it is used for three of the
270 conserved sites and three of the common variable sites (Fig. 7B). The temporal analysis showed
271 that most avian N2s carry five sites, whereas the swine and human N2 head domains increased
272 from five to six and seven sites in the more recent H3N2 isolates (Fig. 7C). These observations
273 suggest that N2s may require more head domain glycans for folding; can accommodate more

274 glycans on the head domain; and/or that the N2 head domain is under more selection pressure
275 than N1.

276

277 *Contributions of the N2 head glycan sites to viral replication, incorporation and stability*

278 To examine the functional contributions of the N2 head glycosylation sites, several mutants
279 were created using a NA (N2-KA17) from a recently recommended H3N2 vaccine strain
280 (A/Kansas/14/2017) and rescued with a WSN backbone. Following passaging in eggs, lower
281 HAU titres and NA activity levels were obtained for the viruses containing the N2-KA17
282 mutants with either the four conserved head glycosylation sites (CHG 2Q) or the two variable
283 glycosylation sites (VHG 4Q) at Asn245 and Asn367, and these values decreased further with
284 the no head glycosylation site (NHG 6Q) mutant (Fig. 7D). Upon analysis of the isolated virions,
285 oxidized N2-KA17 dimers were readily apparent for WT that can be reduced by DTT (Fig. 7E).
286 Similar faster migrating bands were observed for the CHG 2Q and VHG 4Q mutants, but the
287 band corresponding to the NHG 6Q mutant was faint. In line with these results, the viruses
288 carrying the CHG 2Q and VHG 4Q mutants possessed ~50% of the NA activity levels found
289 in the virus containing N2-KA17 WT, whereas the NHG 6Q mutant virus possessed ~35% (Fig.
290 7E). Based on the relatively high retention of N2 when the head glycan sites were absent, we
291 examined the stability of the N2 mutants. In contrast to N1, the thermostability of N2 did not
292 significantly change upon removal of the head glycans (Fig. 7F), indicating that glycan addition
293 and removal has a more minimal structural impact on N2.

294

295 **DISCUSSION**

296 In this study, sequence-based analyses were combined with several experimental approaches to
297 examine the potential functions of the *N*-linked glycans on NA from H1N1 and H3N2 IAVs.
298 Our results show that three glycosylation sites (Asn88, Asn146 and Asn235) are well-conserved
299 on the N1 head domain and that N2 possesses four conserved sites (Asn86, Asn146, Asn200
300 and Asn234), which are similar in position. Based on the available sequences, it appears that
301 variable glycosylation sites on the NA head domain are primarily found on human H1N1 IAV
302 strains and that nucleotide substitutions, insertions and/or deletions are likely responsible for
303 the temporal nature of these sites, together with reassortant events involving the NA gene
304 segment [39-41]. In contrast, the variable sites on the NA head domain in H3N2 strains are not
305 exclusive to the species of origin and these mainly appear to result from nucleotide substitutions.
306 Despite the position conservation, none of the head domain glycosylation sites were essential
307 for viral replication in MDCK cells, or eggs, indicating IAVs would not be significantly

308 impacted by inefficient recognition of these sites. In line with a potential role in NA maturation
309 [21], viral growth defects were observed when all the conserved sites on the NA head domain
310 were absent and these coincided with a decrease in the virion incorporation of NA. However,
311 NA activity was detected in all the viruses containing mutations in the head glycosylation sites,
312 indicating a portion of NA can properly mature when one or more of the conserved head domain
313 sites are absent, raising the question of why these sites are conserved in nature.

314
315 Although the results primarily focused on H1N1 and H3N2 IAVs, we also found that the
316 conserved glycosylation sites on the N1 head domain (Asn88, Asn146 and Asn235) are also
317 highly prevalent in avian and swine IAV strains carrying a HxN1 subtype combination, where
318 x is any of the other sixteen HA subtypes. In addition, the conserved sites in the N2 head domain
319 (Asn86, Asn146, Asn200 and Asn234) also exist at a high frequency in human H2N2 strains,
320 swine HxN2 and avian HxN2 strains, but in the latter two, lower conservation was observed for
321 the Asn86 and Asn234 sites. However, only the Asn146 site is conserved in all other avian NA
322 subtypes (N3-N9), and the highly prevalent sites in the head domains of these subtypes vary in
323 number from two to five and in position, indicating the function of NA head glycans may differ
324 between subtypes.

325
326 Inefficient recognition of the glycosylation sites may be one reason why multiple sites are
327 conserved, as growth defects were only clear when multiple conserved glycan sites were absent.
328 Along these lines, some H1N1 strains that lack one of the three conserved head glycosylation
329 sites have been found, and only the Asn146 site is the more efficiently recognized sequence N-
330 X-T in H1N1 IAVs and is also present in all other NA subtypes at this position [43]. However,
331 three of the conserved N2 head domain sites contain the N-X-T sequence (Asn146, Asn200 and
332 Asn234) and the gel shifts that were observed indicate the different sites are generally
333 recognized. These observations suggest that the individual sites could provide a subtle increase
334 in the replication efficiency of H1N1 IAVs that was not detected by our assays, but it is equally
335 plausible that the conserved sites provide a growth or immunogenicity advantage *in vivo*, as has
336 been reported for several other viral glycoproteins [45-47].

337
338 In support of a possible role *in vivo*, the two N-X-T sites on the N1 head domain (Asn146 and
339 Asn434) both affected the enzymatic properties and the conserved site at Asn146 has previously
340 been reported to possess a unique, wide array, of branched glycan structures [35]. The sites are
341 also proximal to one another and near the central Ca²⁺ binding site on top of the N1 tetramer,

342 indicating the glycan or the site may alter the conformation dependent affinity for this Ca²⁺,
343 which is a major NA stability determinant [26]. In line with this interpretation, less significant
344 stability affects were observed when the variable N-X-T site was inserted into a N1 (NA/CA09)
345 with a lower central Ca²⁺ binding site affinity (data not shown). Currently, we cannot investigate
346 the structural consequence of the insertion more directly because no structure is available for a
347 human N1 head domain between 1948-2009, which contains the amino acid insertion resulting
348 in the additional glycosylation site.

349
350 An interesting observation is that N1 sequences predominantly utilize the N-X-S consensus
351 glycosylation site, whereas N2 sequences are significantly biased towards N-X-T sites and
352 some sites show species specific X residues. This suggests that recognition is more critical for
353 N2 than N1, and that the conserved N1 sites are required for a specific function such as limiting
354 epitope access. However, an enzyme-linked lectin (ELLA) analysis [48] of viruses containing
355 N1-NY09 with and without the insertion and Asn434 glycan addition showed no difference in
356 reactivity to a ferret antiserum raised against an NA (N1-CA09) almost identical to N1-NY09.
357 Conversely, N1-WA01 did not gain reactivity against the same antiserum when the deletion
358 was introduced, indicating that the antigenic changes between these two strains is not related to
359 the removal or addition of the Asn434 glycosylation site in the human N1 head domain (data
360 not shown). While this was somewhat surprising, the region surrounding the central Ca²⁺-
361 binding site on the N1 tetramer has previously been shown to be highly conserved [26],
362 indicating that it may not be subject to significant selection pressure or that antibodies binding
363 to this region do not negatively impact viral replication.

364
365 Assigning functions to *N*-linked glycans on viral glycoproteins is difficult, as a role in
366 maturation does not exclude an additional role in altering surface epitopes. The observation that
367 the number of glycan sites on the N1 head domain have both increased and decreased over time,
368 whereas those on N2 have primarily increased in number, suggests that glycan site addition
369 may have subtype-dependent effects. Supporting this possibility, N2 has a higher prevalence of
370 head glycosylation sites and variable sites, and the N1 variable site at Asn386, which was
371 introduced during the 2009 pandemic, was quickly lost in the circulating strains. There also are
372 additional glycosylation sites with a low frequency in the database that we did not examine,
373 indicating some may be advantageous in specific populations. In this study, we demonstrated
374 that the glycosylation sites on the NA head domain are required for efficient virion
375 incorporation and replication, indicating mutations in these sites are likely useful for creating

376 attenuated IAV strains. These mutant strains can also be used for future studies examining how
377 the conserved N-linked glycan sites on NA contribute to IAV viability, antigenicity, antibody
378 binding and transmissibility in addition to their likely function during maturation.

379

380 **MATERIALS AND METHODS**

381 *Reagents and antibodies*

382 Dulbecco's Modified Eagles Medium (DMEM), fetal bovine serum (FBS), L-glutamine,
383 penicillin/streptomycin (P/S), Opti-MEM (OMEM), anti-goat IgG HRP-linked secondary
384 antibody, Simple Blue Stain, Novex 4-12% Tris-Glycine SDS-PAGE gels, lipofectamine and
385 dithiothreitol (DTT) were all purchased from Thermo Fisher Scientific. 2'-(4-
386 methylumbelliferyl)- α -D-N-acetylneuraminic acid (MUNANA) was obtained from Cayman
387 Chemical. Anti-rabbit IgG HRP-linked secondary antibody and 0.45- μ m polyvinylidene
388 difluoride (PVDF) membrane were obtained from GE healthcare. Specific-Pathogen-Free (SPF)
389 eggs and turkey red blood cells (TRBCs) were purchased from Charles River Labs and the
390 Poultry Diagnostic and Research Center (Athens, GA), respectively. Rabbit antisera against
391 NA was generated by Agrisera (Sweden) using NA-WSN33 residues 35–453 isolated from *E.*
392 *coli* inclusion bodies. Polyclonal goat antisera against influenza virus HAs from
393 A/California/04/2009 (NR-15696) and A/Fort Monmouth/1/1947 (NR-3117) were both obtained
394 from BEI Resources, NIAID, NIH.

395

396 *Plasmids and constructs*

397 The eight reverse genetics (RG) plasmids encoding the PR8 and WSN33 gene segments were
398 provided by Dr. Robert Webster (St. Jude Children's Research Hospital). The RG plasmid
399 containing NA (N1-NY09) from the H1N1 strain A/New York/18/2009 was described
400 previously [26]. The NA gene segments from the strains A/Waikato/7/2001 (N1-WA01),
401 A/Michigan/45/2015 (N1-MI15), A/Kansas/14/2017 (N2-KA17) and the CHG 2Q, VHG 4Q,
402 and NHG 6Q were all synthesized (Eurofins Genomics or GeneScript) and used to generate the
403 RG plasmids as follows. The pHW2000 plasmid back bone [49] and the NA gene segments
404 were amplified by PCR using forward and reverse primers (Table 1) with complementary NA
405 5' and 3' UTR overhangs that direct the recombination upon transformation into *E. coli* [50].
406 The N1-BR18 RG plasmid was generated by cloning the NA gene segment from the H1N1
407 strain A/Brisbane/02/2018 IVR-190 grown in SPF eggs into the plasmid pHW2000 following
408 PCR amplification [51]. Mutations in the N1-MI15 head domain (S90A, S90P, T148A and
409 lineN235K) and the N1-BR18 head domain (N86Q, N146Q and N235), codon insertions in N1-

410 NY09 (+435T and +436A), codon deletions in N1-WA01 (-435T and -437I), and the
 411 substitutions in N1-NY09 (I436T) and N1-WA01 (T436A) were all made with site-directed
 412 mutagenesis primers (Table 2) using the respective NA RG plasmid as a template. All
 413 constructs were confirmed by sequencing (Eurofins MWG Operon or the FDA core facility).
 414

NA or plasmid	Forward primer 5' to 3'	Reverse primer 5' to 3'
N1-WA01	GAAGTTGGGGGGAGCAAAGCAGGAGTTTAAATGAATC	GGTTATTAGTAGAAACAAGGAGTTTTTCAACGGAC
N1-MI15	CGACCTCCGAAGTTGGGGGGAGCAAAGCAGGAGTTTAAATGAATC	CATTTTGGGCCGCCGGTTATTAGTAGAAACAAGGAGTTTTTGAAC
N1-BR18	TATTCGTCTCAGGGAGCAAAGCAGGAGT	ATATCGTCTCGTATTAGTAGAAACAAGGAGTTTTT
N2-KA17	CGACCTCCGAAGTTGGGGGGAGCAAAGCAGGAGTG	CATTTTGGGCCGCCGGTTATTAGTAGAAACAAGGAG
pHW2000	CCTTGTTTCTACTAATAACC	CCTGCTTTTGCTCC

415 **Table 1. Primers used for inserting the NA gene segments into the pHW2000 plasmid**

416

NA	Mutation	Forward primer 5' to 3'	Reverse primer 5' to 3'
N1-MI15	S90A	GCAATTCGCTCTCTGCCCTG	CAGGGCAGAGAGCGGAATTGC
N1-MI15	S90P	GCAATTCCTCTCTCTGCCCTG	CAGGGCAGAGAGGGGAATTGC
N1-MI15	T148A	CATTCCAATGGAGCCATTAAAGACAGG	CCTGTCTTTAATGGCTCCATTGGAATG
N1-MI15	N235K	GTGCATGTGTAAGGTTCTTGCTTTACC	GGTAAAGCAAGAACCCTTTACACATGCAC
N1-BR18	N88Q	CGTGAAATTAGCGGGCCAGTCTCTCTCTGCCCTG	CAGGGCAGAGAGAGGACTGGCCCGCTAATTTACG
N1-BR18	N146Q	TTGCTAAATGACAAACATTCCCAGGGAACATTAAAGACAGGAGC	GCTCCTGTCTTTAATGGTCCCTGGGAATGTTTGTCATTTAGCAA
N1-BR18	N235Q	GAGTCTGAATGTGCATGTGTACAGGGTTCTTGCTTTACCATAATG	CATTATGGTAAAGCAAGAACCCTGTACACATGCACATTCAGACTC
N1-NY09	I436T	GAGAACACAACCTGGACTAGCGGGAGCAG	GCTAGTCCAGGTTGTGTTCTCTTTGGGTCG
N1-NY09	+435T	AAAGAGAACACAACAATCTGGACTAGCGGGAGC	CCAGATTGTTGTGTTCTCTTTGGGTCGCTC
N1-NY09	+436A	GAGAACACAGCTATCTGGACTAGCGGGAGC	AGTCCAGATAGCTGTGTTCTCTTTGGGTCG
N1-WA01	T436A	AGAAAATACAGCAATCTGGACTAGTGGGAGC	TCCAGATTGCTGTATTTCTTTGGCAGTCC
N1-WA01	-435T	AAAAGAAAATACAATCTGGACTAGTGGAGC	TCCAGATTGTATTTCTTTGGCAGTCC
N1-WA01	-437I	AGAAAATACAACATGGACTAGTGGGAGCAGC	TAGTCCATGTTGTATTTCTTTGGCAGTCC

417 **Table 2. Primers used for introducing the site-directed mutations in the NA head domain**

418

419 *Cell culture and viral reverse genetics*

420 Madin-Darby canine kidney 2 (MDCK.2; CRL-2936) cells and HEK 293T/17 cells (CRL-
 421 11268), obtained from LGC Standards, were cultured in DMEM containing 10% FBS and
 422 100 U/ml of P/S in a 37 °C atmosphere with 5% CO₂ and ~95% humidity. Reassortant viruses
 423 carrying N1-MI15, N1-NY09 or N1WA01 variants were generated by 8-plasmid reverse
 424 genetics using the indicated NA and the complimentary seven ‘backbone’ gene segments of
 425 WSN33 as previously described [26]. Reassortant viruses carrying N1-BR18 or N2-KA17
 426 variants were generated by 8-plasmid reverse genetics using the seven ‘backbone’ gene
 427 segments of WSN33 or PR8 as follows using 6-well plates. One day prior, 1.2x10⁶ 293T cells
 428 and 1.2x10⁶ MDCK.2 cells were plated per well using 3 ml DMEM with 10% FBS. The next

429 day, the medium was replaced with 2 ml of OMEM, the eight plasmids were added to 200 μ l
430 of OMEM at a concentration of 1 μ g per plasmid, combined with 18 μ l of lipofectamine and
431 the mixture was incubated 45 min at room temperature. The cell medium was removed, the
432 mixture was added to one well and the dish was incubated 5 min at 37 °C before 800 μ l
433 OMEM was added to each well. Approximately 24 h post-transfection 1ml OMEM
434 containing 4 μ g/ml TPCK trypsin was added to each well. Culture medium was harvested
435 between 72-96 h post-transfection, clarified by centrifugation (2000 \times g; 5 min) and passaged
436 using SPF eggs or MDCK.2 cells.

437

438 *Viral Passaging in MDCK.2 cells and SPF eggs*

439 For cell passaging, one day after seeding 1×10^6 MDCK.2 cells on a 6 cm dish, the culture
440 medium was removed, and the cells were washed with 1 ml infection medium (IM) comprised
441 of DMEM, 0.3% BSA, 0.1% FBS, and P/S. Each dish then received 2 ml of cold IM
442 containing 10 μ l of the clarified viral reverse genetics medium and was rocked at 4 °C for 30
443 min. The inoculation medium was then removed, cells were washed with 1 ml of IM, 5 ml of
444 IM containing 10 μ g/ml TPCK-trypsin was added and the dish was placed at 37 °C. The
445 culture medium was harvested at the peak of cytopathic effects (~48-72 h post-infection) and
446 clarified by centrifugation (2000 \times g; 5 min) prior to analysis, storage, or sedimentation.

447 Passaging in SPF eggs was carried out by inoculating 100 μ l of clarified viral reverse genetics
448 medium into 9-11 day old embryonated eggs and incubating them for 3 days at 33 °C.

449 Following the incubation, eggs were chilled at 4 °C for 2 h and the allantoic fluid from each
450 egg was harvested, clarified by centrifugation (2000 \times g; 5 min) and stored in aliquots at -
451 80 °C. Viruses in the allantoic fluid from the first passage were then diluted (1:1000) in sterile
452 PBS and 100 μ l was used to inoculate the 9-11 day old embryonic eggs. For each virus,
453 groups of eight or seven eggs were used, the allantoic fluid from each egg was harvested
454 individually and clarified by centrifugation (2000 \times g; 5 min) prior to analysis or
455 sedimentation.

456

457 *Viral sedimentation and sucrose gradient isolation*

458 Clarified virus-containing culture medium (~8 ml) or allantoic fluid (~28 ml) were added to
459 ultracentrifuge tubes and a sucrose cushion (25% w/v sucrose, PBS pH 7.2 and 1 mM CaCl₂)
460 equal to ~15% of the sample volume was layered under each sample. Virions were then isolated
461 by sedimentation (100,000 \times g; 45 min) at 4 °C and the supernatant was aspirated. Cell

462 produced viral pellets were resuspended in 200 μ l PBS pH 7.4 and 1 mM CaCl_2 and NA activity
463 was analysed prior to immunoblotting. Egg produced virions were resuspended in 200 μ l of
464 PBS pH 7.2 containing 1 mM CaCl_2 . For sucrose gradient isolations, the resuspension solution
465 containing 12.5% w/v sucrose was layered on top of a discontinuous gradient containing four
466 8.5 ml sucrose layers (60% w/v, 45% w/v, 30% w/v and 15% w/v sucrose in PBS pH 7.2 and 1
467 mM CaCl_2) and centrifuged at $100,000 \times g$ for 2 h at 4 °C. Fractions were isolated from top to
468 bottom, the density was determined with a refractometer and those corresponding to 30-50%
469 w/v sucrose were pooled, mixed with 2 volumes of PBS pH 7.2 and 1 mM CaCl_2 , and the
470 virions were sedimented ($100,000 \times g$; 45 min). The supernatant was discarded, and the viral
471 pellet was resuspended in 250 μ l PBS pH 7.2 containing 1 mM CaCl_2 . Total protein
472 concentrations in resuspended viral pellets were all determined with a BCA protein assay kit
473 (Pierce) using the 96-well plate protocol. The average value was determined from the 1:2 and
474 1:4 sample dilutions and each sample was adjusted to a final concentration of 1 mg/ml using
475 PBS pH 7.2 containing 1 mM CaCl_2 .

476

477 *HAU titre, NA activity and thermostability measurements*

478 HAU titres were determined using a 96-well plate and 0.5% TRBCs in PBS pH 7.2. Briefly,
479 90 μ l of PBS pH 7.2 was added to the first column and 50 μ l to remaining columns. From
480 each infected egg, 10 μ l of allantoic fluid was added to the first column creating a 1:10
481 dilution. A two-fold serial dilution was made by transferring 50 μ l from each column to the
482 subsequent column and 50 μ l of 0.5% TRBCs were added to each well. The plate was
483 incubated 30 min at room temperature and the HAU titre was determined as the last well
484 where agglutination was observed. For sialidase activity measurements, equal amounts of
485 clarified virus-containing medium, allantoic fluid or sedimented viral samples were brought
486 up to 195 μ l in reaction buffer (0.1 M KH_2PO_4 pH 6.0 and 1 mM CaCl_2), transferred to a 96-
487 well black clear bottom plate (Corning) and incubated at 37 °C for 15 min. Reactions were
488 then initiated by adding 5 μ l of 2 mM MUNANA and the fluorescence was measured with
489 either a SpectraMax Gemini EM plate reader or a Cytation 5 (Biotek) using 365 nm excitation
490 and 450 nm emission wavelengths. NA thermostability was determined by exposing equal
491 amounts of clarified virus-containing media to temperatures ranging from 37 °C to 64 °C for
492 10 min and measuring the residual sialidase activity as previously described [26].

493

494 *SDS-PAGE, Coomassie staining and immunoblotting,*

495 Sedimented viral samples containing equal resuspension volumes or the indicated total protein
496 amounts were mixed with Laemmli sample buffer that contained 0.1M DTT as indicated.
497 Samples were then heated 37 °C or 50 °C for 10 min and resolved by either 7.5 % (α -NA), 11 %
498 (α -HA) or 4-12 % (α -NA, α -HA and Coomassie) Tris-Glycine SDS-PAGE gels. Gels were
499 Coomassie stained using simple blue or transferred to a 0.45- μ m pore PVDF membrane at 15
500 V for 1 h. PVDF membranes were blocked with milk/PBST (3% nonfat dry milk, PBS, pH 7.4,
501 0.1% Tween 20) for 30 min and processed using standard immunoblotting protocols with the
502 indicated antibodies and the appropriate HRP-linked secondary antibody. Immunoblots were
503 developed with the SuperSignal West Femto kit (ThermoFischer) and imaged using an Azure
504 C600 or a Syngene G Box.

505

506 *Analysis of NA glycosylation sites and in silico glycosylation models*

507 Complete NA protein sequences from H1N1 and H3N2 IAVs of human, avian and swine
508 origin were downloaded from The Influenza Virus Resource at the National Center for
509 Biotechnology Information [52]. Each group was aligned using MAFFT v7.311 with default
510 progressive method (FFT-NS-2). Mislabeled sequences were manually removed. The final
511 NA data sets consist of 18966 sequences from human H1N1 strains (1918-2019/11/20), 630
512 sequences from avian H1N1 strains (1976-2018/11/16), 4949 sequences from swine H1N1
513 strains (1930-2019/12/20), 24184 sequences from human H3N2 strains (1968-2019/11/09),
514 411 sequences from avian H3N2 strains (1969-2018/10/13), and 3484 sequences from swine
515 H3N2 strains (1970-2019/12/19). Potential glycosylation sites (N-X-S/T-X), where X
516 represents every amino acid except for Pro, were located using a Python script. N1 2009
517 pandemic-like amino acid numbering was used for both N1 and N2, the head domain was set
518 to begin at amino acid residue 82 and the stalk was designated as amino acid residues 35 to
519 81. Tetrameric N1 models were created from the A/Michigan/45/2015 primary sequence
520 using SWISS-MODEL (<https://swissmodel.expasy.org>), based on an available 2009
521 pandemic-like N1 head domain structure (PDBID: 5NWE) [53], and the glycans were added
522 *in silico* using Glyprot (<http://www.glycosciences.de/modeling/glyprot/php/main.php>). The
523 modeled glycan structures were chosen based on previous work [35] with glycan number
524 9141 (glcp) being used for Asn386 and 8714 (2 glcnac) for all other sites.

525

526

527

528

529 **FIGURE LEGENDS**

530

531 **Figure 1. N-linked glycan site variation in NA from H1N1 IAVs by species of origin and**

532 **time. A.** Diagram of an N-linked glycan structure that is transferred to secretory glycoproteins

533 during entry into the ER lumen. The glycan is added to the Asn (N) of the consensus sequence

534 N-X-S/T. **B.** Linear and structural organization of the domains in NA from H1N1 IAVs. The

535 numbers correspond to the amino acid position at the start of the transmembrane (TM), stalk

536 and head domains of these NAs. **C.** Graphs showing the prevalence of the N1 sequences from

537 human (n=18966), swine (n=4949), and avian (n=630) H1N1 IAVs that possess the indicated

538 number of glycosylation sites in the stalk and head domain (**left panel**), the stalk alone

539 (**middle panel**) and the head domain alone (**right panel**). **D.** Temporal graphs displaying the

540 mean number of glycosylation sites in the N1 head domain with respect to the year the avian

541 (**left panel**), swine (**middle panel**), and human (**right panel**) H1N1 IAVs were isolated.

542 Filled circles correspond to the mean. Lines show the range in the number of sites in the

543 sequence set for each year. All analyses were performed using full-length NA sequences

544 downloaded from the NCBI Influenza Database.

545 **Figure 2. Positions of the N-linked glycan sites in the NA head domain from H1N1 IAVs.**

546 **A.** Graph showing the prevalence of the most frequent head domain glycosylation sites in the

547 N1 sequences based on the H1N1 IAV species of origin. The positioning refers to the Asn (N)

548 in the N-X-S/T sequence. **B.** *In silico* model of N-linked glycan structures mapped onto the

549 conserved sites of a 2009 pandemic-like N1 head domain structure (PDBID: 5NWE) [53]. **C.**

550 Temporal graphs displaying the frequency of the most prevalent variable glycosylation sites in

551 the head domain of N1 with respect to the year the sequences were isolated. **D.** *In silico* model

552 of N-linked glycans mapped onto a N1 head domain structure (PDBID: 5NWE) [53] at amino

553 acids that correspond to the position of the prevalent variable head glycosylation sites.

554

555 **Figure 3. The conserved N1 head glycosylation sites are not essential for viral replication**

556 **in cells. A.** Logo plots displaying the amino acid (top) and nucleotide (bottom) frequency for

557 the three conserved glycosylation sites on the N1 head domain from human H1N1 IAVs. **B and**

558 **C.** Representative NA and HA immunoblots of recombinant WSN viruses carrying N1-MI15

559 with the indicated glycosylation site mutations. The viruses were rescued by reverse genetic,

560 passaged in MDCK cells and the viral-containing supernatants were sedimented and

561 resuspended in equal volumes. Each sample was split, one part was resolved by non-reducing

562 (NR) SDS-PAGE prior to immunoblotting, and the other was used to determine the NA activity

563 values, which are listed below the blots. Samples (C) containing resuspension volumes greater
564 than the WT control are indicated as a ratio in the parenthesis.

565

566 **Figure 4. Mutation of the conserved N1 head glycosylation sites causes slight viral**
567 **replication defects in eggs. A.** Scatter plots of the HAU titers and NA activities that were
568 measured in the allantoic fluid harvested from eggs infected with recombinant PR8 viruses
569 carrying N1-BR18 with the indicated glycosylation site mutations. The viruses were rescued
570 by reverse genetics and passaged twice in eggs. The data points from individual eggs following
571 the second passage are shown together with the median (line). *P* values (95% CI) were
572 determined with respect to the WT values by a one-way ANOVA. **B.** Representative NA and
573 HA immunoblots of the recombinant PR8^{N1-BR18} viruses with the indicated mutations in the N1
574 head glycosylation sites. The allantoic fluid from the second passage was pooled, the virions
575 were isolated by centrifugation and adjusted to equal total protein concentration prior to being
576 resolved by NR and reducing (RD) SDS-PAGE. NA activity (below the immunoblots) in the
577 virions was also measured using equal total protein amounts.

578

579 **Figure 5. N1 viral incorporation is reduced when the conserved head glycosylation sites**
580 **are absent. A.** Scatter plots of the HAU titers and NA activities in the allantoic fluid harvested
581 from eggs infected with recombinant WSN viruses carrying N1-BR18 (WT) or N1-BR18 with
582 no head glycan sites (NHG 3Q), which was generated by Gln mutations of each head
583 glycosylation site (N88Q, N146Q and N235Q). The viruses were rescued by reverse genetics
584 and passaged twice in eggs. The data points from individual eggs following the second passage
585 are shown with the median. *P* values (95% CI) are from a two-tailed unpaired t-test. **B.**
586 Representative image of a Coomassie stained SDS-PAGE gel containing the indicated
587 recombinant WSN^{N1-BR18} viruses. The allantoic fluid from a second passage in eggs was pooled,
588 the virions were isolated by centrifugation, and the protein concentration was determined.
589 Samples containing ~5µg of total protein were treated with the reductant DTT as indicated and
590 resolved using a 4-12% Tris-glycine SDS-PAGE gel. Inter- (N1-BR18^{OX}) and intra- (HA^{OX})
591 molecular disulfide bonded NA and HA are indicated along with the reduced forms (N1-
592 BR18RD, HA1, and HA2). The viral proteins NP and M1 are also indicated. The NA activity
593 listed below the gel was measured using equal total protein amounts of the two viruses. **C.** NA
594 and HA immunoblots of the isolated recombinant WSN^{N1-BR18} viruses. Samples containing
595 equal total protein amounts were treated with DTT as indicated, resolved using a 4-12% Tris-
596 glycine SDS-PAGE gel and transferred to a PVDF membrane prior to immunoblotting.

597

598 **Figure 6. N1 stability decreases from the head domain insertion that creates the variable**
599 **Asn434 glycosylation site. A.** Logo plots displaying the amino acid (top) and nucleotide
600 (bottom) frequency for the three N-X-S variable glycosylation sites on the N1 head domain
601 from human H1N1 IAVs. **B.** Amino acid (top) and nucleotide (bottom) logo plot for the N-X-
602 T variable glycosylation site in the N1 head domain from human H1N1 IAVs. A timeline
603 showing when the insertion and the necessary mutations appeared in the database is included
604 to the right. Note that the N1 ‘insertion’ was lost in 2009 when the pandemic H1N1 IAV of
605 swine origin became prevalent. **C and D.** Representative NA and HA immunoblots of
606 recombinant WSN viruses carrying (C) N1-NY09 with the indicated mutations and insertions
607 or (D) N1-WA01 with the indicated mutations and deletions. The viruses were rescued by
608 reverse genetic, passaged in MDCK cells and the viral-containing supernatants were
609 sedimented, resuspended in equal volumes and resolved by NR SDS-PAGE. **E.** NA T_{50}
610 temperatures are displayed for the recombinant WSN viruses carrying N1-NY09 or N1-WA01
611 with the indicated mutations, insertions or deletions. The measurements ($n = 3$ biologically
612 independent experiments) were taken in tissue culture medium with the NA activity at 37°C set
613 to 100%. The line represents the mean. **F.** NA T_{50} temperatures are displayed for the WSN
614 reassortant viruses carrying N1-MI15 with the indicated glycan site mutations. The
615 measurements ($n = 4$ biologically independent experiments) were taken in tissue culture
616 medium with the NA activity at 37°C set to 100%. The line depicts the mean and the P values
617 (95% CI) were determined with respect to WT by a one-way ANOVA.

618

619 **Figure 7. Variation in the NA glycan sites from H3N2 IAVs by species of origin and time.**
620 **A.** Graphs showing the prevalence of the NA sequences from human ($n=24184$), swine
621 ($n=3484$), and avian ($n=411$) H3N2 IAVs that possess the indicated number of glycosylation
622 sites in the N2 stalk and head domain (**left panel**), the stalk alone (**middle panel**) and the head
623 domain alone (**right panel**). **B.** The prevalence of the most frequent glycosylation sites in the
624 N2 head domain sequences is shown based on the H3N2 IAV strain species origin. The glycan
625 site position refers to the Asn (N) in the N-X-S/T sequence. Sites with an N-X-T sequence have
626 an asterisk. **C.** Graphs displaying the mean number of glycosylation sites in the N2 head domain
627 with respect to the year the avian (**left panel**), swine (**middle panel**), and human (**right panel**)
628 H3N2 IAVs were isolated. Filled circles correspond to the mean and lines show the range in
629 the site number for the sequence sets from each year. Sequences were obtained from the NCBI

630 Influenza Database. **D.** Scatter plot of the HAU titers and NA activities from the allantoic fluid
631 of individual eggs infected with recombinant WSN viruses carrying N2-KA17 (WT) or mutants
632 that contain only the conserved head glycan sites (CHG 2Q), variable head glycan sites (VHG
633 4Q), or no head glycan sites (NHG 6Q). Data from the second passage is shown with the median.
634 *P* values (95% CI) were determined with respect to WT by a one-way ANOVA. **E.** The
635 indicated recombinant WSN^{N2-KA17} viruses were isolated from allantoic fluid by centrifugation,
636 separated by SDS-PAGE, and visualized by Coomassie staining. Prior to loading ~5µg of total
637 protein was treated or untreated with DTT. The NA activity for each virus was measured using
638 equal protein amounts. Asterisks mark bands corresponding to N2-KA17 dimers and tetramers
639 (-DTT) or reduced monomers (+DTT). **F.** NA *T*₅₀ temperatures were determined for the
640 indicated WSN reassortant viruses in PBS pH 7.2 with 1mM CaCl₂. NA activity at 37°C set to
641 100%. The line is the mean and the *P* values (95% CI) were calculated with respect to WT by
642 a one-way ANOVA.

643 ACKNOWLEDGEMENTS

644 We would like to thank Tahir Malik (FDA), Hongquan Wan (FDA) and Daniel Hebert
645 (University of Massachusetts-Amherst) for critically reading the manuscript and offering
646 several helpful suggestions. This work was supported by in part by grants from the Swedish
647 Research Council K2015-57-21980-04-4 and the Carl Trygger Foundation CTS17:111, as well
648 as federal funds from the NIAID, National Institutes of Health, Department of Health and
649 Human Services, under CEIRS contract number HHSN272201400005C.

650

651 REFERENCES

- 652 1. Mochizuki, K., et al., *Two N-linked glycans are required to maintain the transport activity*
653 *of the bile salt export pump (ABCB11) in MDCK II cells.* Am J Physiol Gastrointest Liver
654 Physiol, 2007. **292**(3): p. G818-28.
- 655 2. Hanson, S.R., et al., *The core trisaccharide of an N-linked glycoprotein intrinsically*
656 *accelerates folding and enhances stability.* Proc Natl Acad Sci U S A, 2009. **106**(9): p.
657 3131-6.
- 658 3. Tokhtaeva, E., et al., *N-glycan-dependent quality control of the Na,K-ATPase beta(2)*
659 *subunit.* Biochemistry, 2010. **49**(14): p. 3116-28.
- 660 4. Hebert, D.N., et al., *The intrinsic and extrinsic effects of N-linked glycans on*
661 *glycoproteostasis.* Nat Chem Biol, 2014. **10**(11): p. 902-10.
- 662 5. Cai, X., et al., *The importance of N-glycosylation on beta3 integrin ligand binding and*
663 *conformational regulation.* SciRep, 2017. **7**(1): p. 4656.
- 664 6. Ohtsubo, K., et al., *Dietary and genetic control of glucose transporter 2 glycosylation*
665 *promotes insulin secretion in suppressing diabetes.* Cell, 2005. **123**(7): p. 1307-21.
- 666 7. Wang, X., et al., *Core fucosylation regulates epidermal growth factor receptor-mediated*
667 *intracellular signaling.* J Biol Chem, 2006. **281**(5): p. 2572-7.

- 668 8. Goetze, A.M., et al., *High-mannose glycans on the Fc region of therapeutic IgG antibodies*
669 *increase serum clearance in humans*. *Glycobiology*, 2011. **21**(7): p. 949-59.
- 670 9. Liu, L., *Antibody glycosylation and its impact on the pharmacokinetics and*
671 *pharmacodynamics of monoclonal antibodies and Fc-fusion proteins*. *J Pharm Sci*, 2015.
672 **104**(6): p. 1866-1884.
- 673 10. Hebert, D.N., B. Foellmer, and A. Helenius, *Glucose trimming and reglucosylation*
674 *determine glycoprotein association with calnexin in the endoplasmic reticulum*. *Cell*, 1995.
675 **81**(3): p. 425-33.
- 676 11. Shi, X. and R.M. Elliott, *Analysis of N-linked glycosylation of hantaan virus glycoproteins*
677 *and the role of oligosaccharide side chains in protein folding and intracellular trafficking*.
678 *J Virol*, 2004. **78**(10): p. 5414-22.
- 679 12. Braakman, I. and E. van Anken, *Folding of viral envelope glycoproteins in the endoplasmic*
680 *reticulum*. *Traffic*, 2000. **1**(7): p. 533-9.
- 681 13. Skehel, J.J., et al., *A carbohydrate side chain on hemagglutinins of Hong Kong influenza*
682 *viruses inhibits recognition by a monoclonal antibody*. *Proc Natl Acad Sci U S A*, 1984.
683 **81**(6): p. 1779-83.
- 684 14. Wei, X., et al., *Antibody neutralization and escape by HIV-1*. *Nature*, 2003. **422**(6929): p.
685 307-12.
- 686 15. Lennemann, N.J., et al., *Comprehensive functional analysis of N-linked glycans on Ebola*
687 *virus GP1*. *mBio*, 2014. **5**(1): p. e00862-13.
- 688 16. Walls, A.C., et al., *Glycan shield and epitope masking of a coronavirus spike protein*
689 *observed by cryo-electron microscopy*. *Nat Struct Mol Biol*, 2016. **23**(10): p. 899-905.
- 690 17. Wan, H., et al., *The neuraminidase of A(H3N2) influenza viruses circulating since 2016 is*
691 *antigenically distinct from the A/Hong Kong/4801/2014 vaccine strain*. *Nat Microbiol*,
692 2019. **4**(12): p. 2216-2225.
- 693 18. Hebert, D.N., et al., *The number and location of glycans on influenza hemagglutinin*
694 *determine folding and association with calnexin and calreticulin*. *Journal of Cell Biology*,
695 1997. **139**(3): p. 613-623.
- 696 19. Daniels, R., et al., *N-linked glycans direct the cotranslational folding pathway of influenza*
697 *hemagglutinin*. *Mol Cell*, 2003. **11**(1): p. 79-90.
- 698 20. Molinari, M., et al., *Contrasting functions of calreticulin and calnexin in glycoprotein*
699 *folding and ER quality control*. *Mol Cell*, 2004. **13**(1): p. 125-35.
- 700 21. Wang, N., et al., *The cotranslational maturation program for the type II membrane*
701 *glycoprotein influenza neuraminidase*. *J Biol Chem*, 2008. **283**(49): p. 33826-37.
- 702 22. Gamblin, S.J. and J.J. Skehel, *Influenza hemagglutinin and neuraminidase membrane*
703 *glycoproteins*. *J Biol Chem*, 2010. **285**(37): p. 28403-9.
- 704 23. Yoon, S.W., R.J. Webby, and R.G. Webster, *Evolution and ecology of influenza A viruses*.
705 *Curr Top Microbiol Immunol*, 2014. **385**: p. 359-75.
- 706 24. Morens, D.M., J.K. Taubenberger, and A.S. Fauci, *The persistent legacy of the 1918*
707 *influenza virus*. *N Engl J Med*, 2009. **361**(3): p. 225-9.
- 708 25. Rajao, D.S., A.L. Vincent, and D.R. Perez, *Adaptation of Human Influenza Viruses to Swine*.
709 *Front Vet Sci*, 2018. **5**: p. 347.
- 710 26. Wang, H., et al., *Structural restrictions for influenza neuraminidase activity promote*
711 *adaptation and diversification*. *Nature Microbiology*, 2019.
- 712 27. Bos, T.J., A.R. Davis, and D.P. Nayak, *NH2-terminal hydrophobic region of influenza virus*
713 *neuraminidase provides the signal function in translocation*. *Proc Natl Acad Sci U S A*,
714 1984. **81**(8): p. 2327-31.
- 715 28. Paterson, R.G. and R.A. Lamb, *Conversion of a class II integral membrane protein into a*
716 *soluble and efficiently secreted protein: multiple intracellular and extracellular oligomeric*
717 *and conformational forms*. *J Cell Biol*, 1990. **110**(4): p. 999-1011.

- 718 29. Bucher, D.J. and E.D. Kilbourne, *A 2 (N2) neuraminidase of the X-7 influenza virus*
719 *recombinant: determination of molecular size and subunit composition of the active unit.* J
720 Virol, 1972. **10**(1): p. 60-6.
- 721 30. Varghese, J.N., W.G. Laver, and P.M. Colman, *Structure of the influenza virus glycoprotein*
722 *antigen neuraminidase at 2.9 Å resolution.* Nature, 1983. **303**(5912): p. 35-40.
- 723 31. Dou, D., et al., *Influenza A Virus Cell Entry, Replication, Virion Assembly and Movement.*
724 *Frontiers in Immunology*, 2018. **9**(1581).
- 725 32. Colman, P.M., J.N. Varghese, and W.G. Laver, *Structure of the catalytic and antigenic sites*
726 *in influenza virus neuraminidase.* Nature, 1983. **303**(5912): p. 41-4.
- 727 33. Nordholm, J., et al., *Polar residues and their positional context dictate the transmembrane*
728 *domain interactions of influenza A neuraminidases.* J Biol Chem, 2013. **288**(15): p. 10652-
729 60.
- 730 34. Dou, D., et al., *Type II transmembrane domain hydrophobicity dictates the cotranslational*
731 *dependence for inversion.* Mol Biol Cell, 2014. **25**(21): p. 3363-74.
- 732 35. She, Y.M., et al., *Topological N-glycosylation and site-specific N-glycan sulfation of*
733 *influenza proteins in the highly expressed H1N1 candidate vaccines.* Sci Rep, 2017. **7**(1):
734 p. 10232.
- 735 36. da Silva, D.V., et al., *Assembly of subtype I influenza neuraminidase is driven by both the*
736 *transmembrane and head domains.* J Biol Chem, 2013. **288**(1): p. 644-53.
- 737 37. da Silva, D.V., et al., *The influenza virus neuraminidase protein transmembrane and head*
738 *domains have coevolved.* J Virol, 2015. **89**(2): p. 1094-104.
- 739 38. Saito, T., G. Taylor, and R.G. Webster, *Steps in maturation of influenza A virus*
740 *neuraminidase.* J Virol, 1995. **69**(8): p. 5011-7.
- 741 39. Sun, S., et al., *Glycosylation site alteration in the evolution of influenza A (H1N1) viruses.*
742 PLoS One, 2011. **6**(7): p. e22844.
- 743 40. Sun, S., et al., *Prediction of biological functions on glycosylation site migrations in human*
744 *influenza H1N1 viruses.* PLoS One, 2012. **7**(2): p. e32119.
- 745 41. Kim, P., et al., *Glycosylation of Hemagglutinin and Neuraminidase of Influenza A Virus as*
746 *Signature for Ecological Spillover and Adaptation among Influenza Reservoirs.* Viruses,
747 2018. **10**(4).
- 748 42. Shakin-Eshleman, S.H., S.L. Spitalnik, and L. Kasturi, *The amino acid at the X position of*
749 *an Asn-X-Ser sequon is an important determinant of N-linked core-glycosylation efficiency.*
750 J Biol Chem, 1996. **271**(11): p. 6363-6.
- 751 43. Mellquist, J.L., et al., *The amino acid following an asn-X-Ser/Thr sequon is an important*
752 *determinant of N-linked core glycosylation efficiency.* Biochemistry, 1998. **37**(19): p. 6833-
753 7.
- 754 44. Eichelberger, M.C. and H. Wan, *Influenza neuraminidase as a vaccine antigen.* Curr Top
755 Microbiol Immunol, 2015. **386**: p. 275-99.
- 756 45. Lavie, M., X. Hanouille, and J. Dubuisson, *Glycan Shielding and Modulation of Hepatitis*
757 *C Virus Neutralizing Antibodies.* Frontiers in Immunology, 2018. **9**(910).
- 758 46. Quinones-Kochs, M.I., L. Buonocore, and J.K. Rose, *Role of N-linked glycans in a human*
759 *immunodeficiency virus envelope glycoprotein: effects on protein function and the*
760 *neutralizing antibody response.* J Virol, 2002. **76**(9): p. 4199-211.
- 761 47. Leemans, A., et al., *Removal of the N-Glycosylation Sequon at Position N116 Located in*
762 *p27 of the Respiratory Syncytial Virus Fusion Protein Elicits Enhanced Antibody Responses*
763 *after DNA Immunization.* Viruses, 2018. **10**(8).
- 764 48. Gao, J., L. Couzens, and M.C. Eichelberger, *Measuring Influenza Neuraminidase Inhibition*
765 *Antibody Titers by Enzyme-linked Lectin Assay.* J Vis Exp, 2016(115).
- 766 49. Hoffmann, E., et al., *A DNA transfection system for generation of influenza A virus from*
767 *eight plasmids.* Proc Natl Acad Sci U S A, 2000. **97**(11): p. 6108-13.

- 768 50. Mellroth, P., et al., *LytA, major autolysin of Streptococcus pneumoniae, requires access to*
769 *nascent peptidoglycan*. J Biol Chem, 2012. **287**(14): p. 11018-29.
- 770 51. Sandbulte, M.R., et al., *A miniaturized assay for influenza neuraminidase-inhibiting*
771 *antibodies utilizing reverse genetics-derived antigens*. Influenza Other Respir Viruses,
772 2009. **3**(5): p. 233-40.
- 773 52. Bao, Y., et al., *The influenza virus resource at the National Center for Biotechnology*
774 *Information*. J Virol, 2008. **82**(2): p. 596-601.
- 775 53. Pokorna, J., et al., *Kinetic, Thermodynamic, and Structural Analysis of Drug Resistance*
776 *Mutations in Neuraminidase from the 2009 Pandemic Influenza Virus*. Viruses, 2018. **10**(7).
777

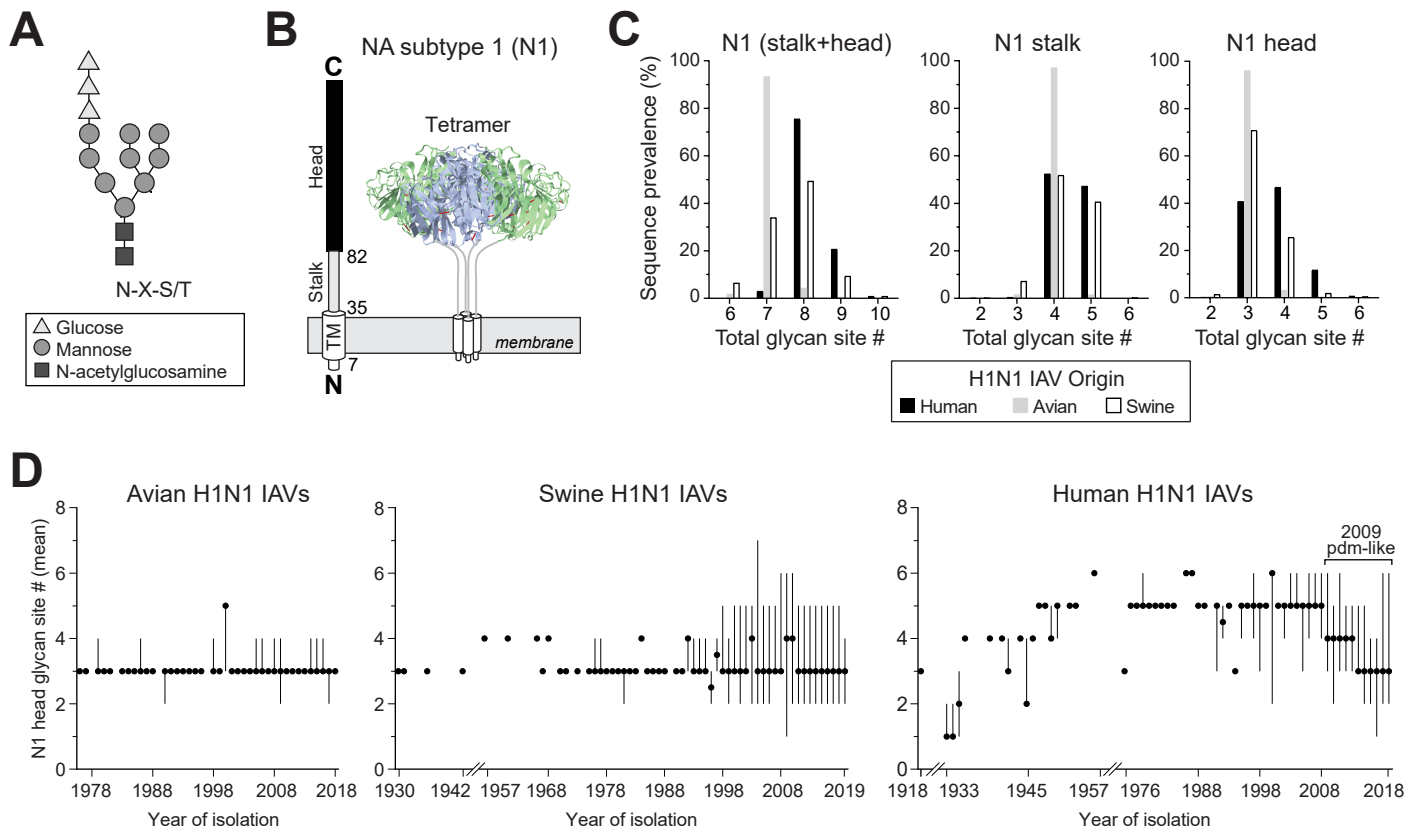


Figure 1

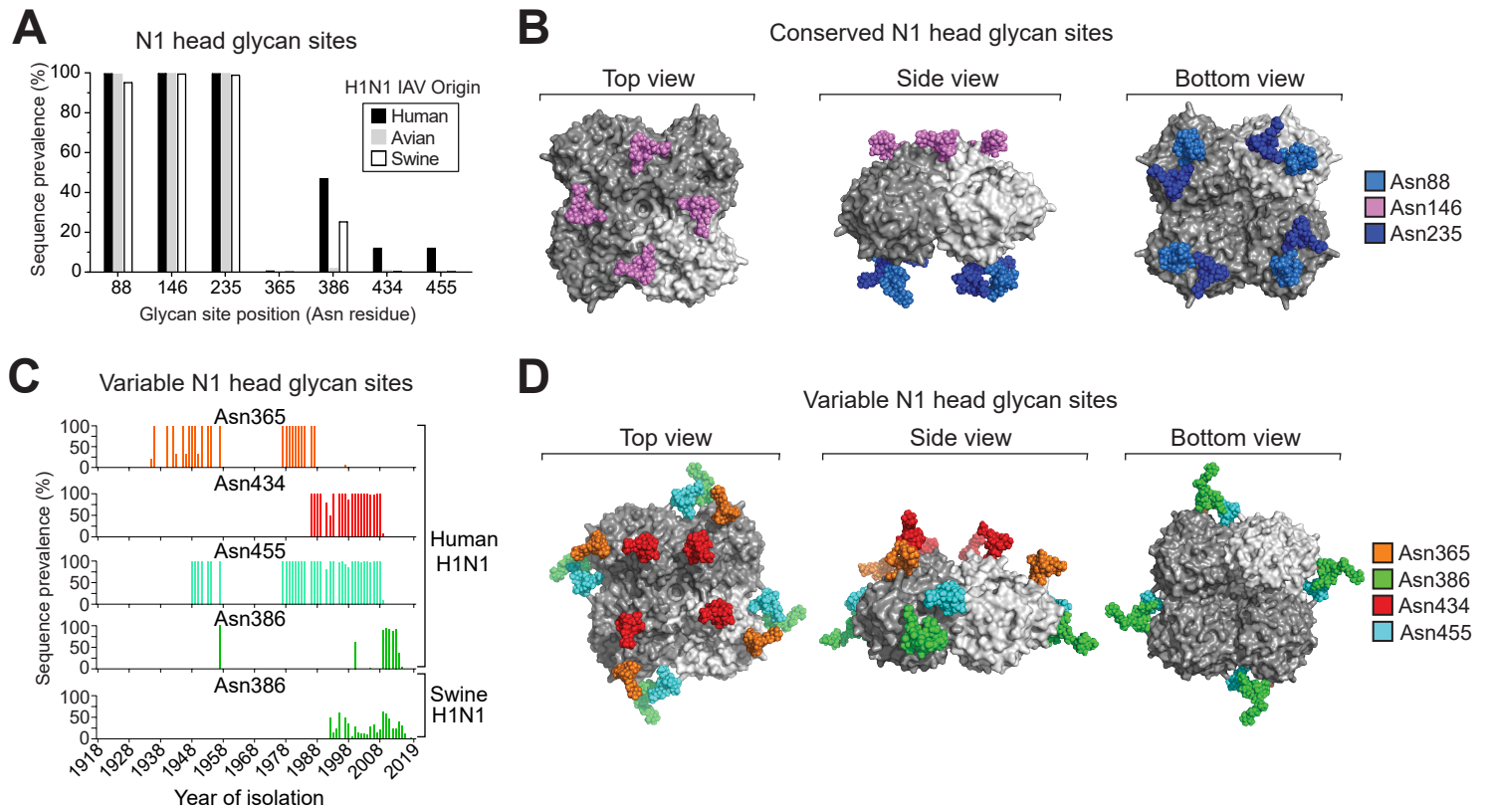


Figure 2

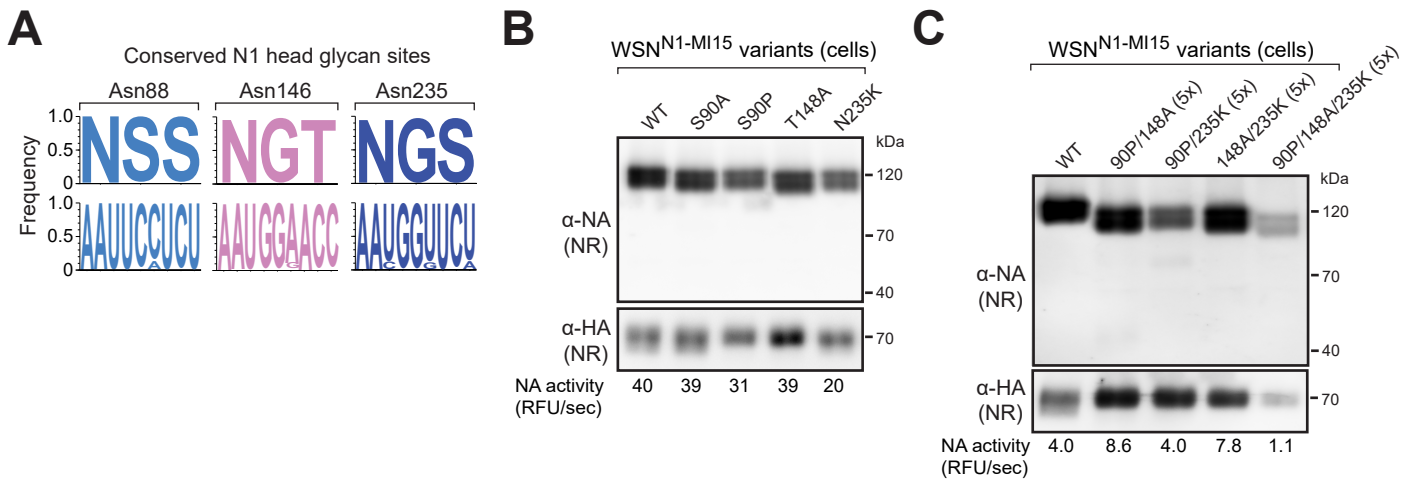


Figure 3

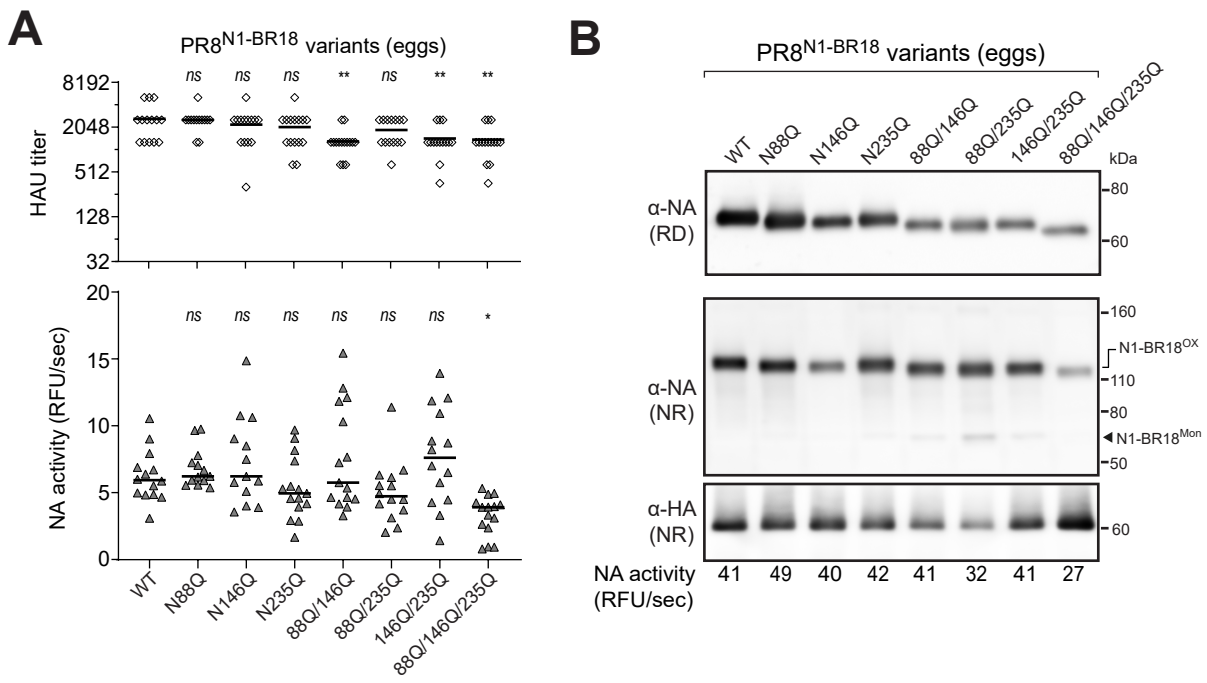


Figure 4

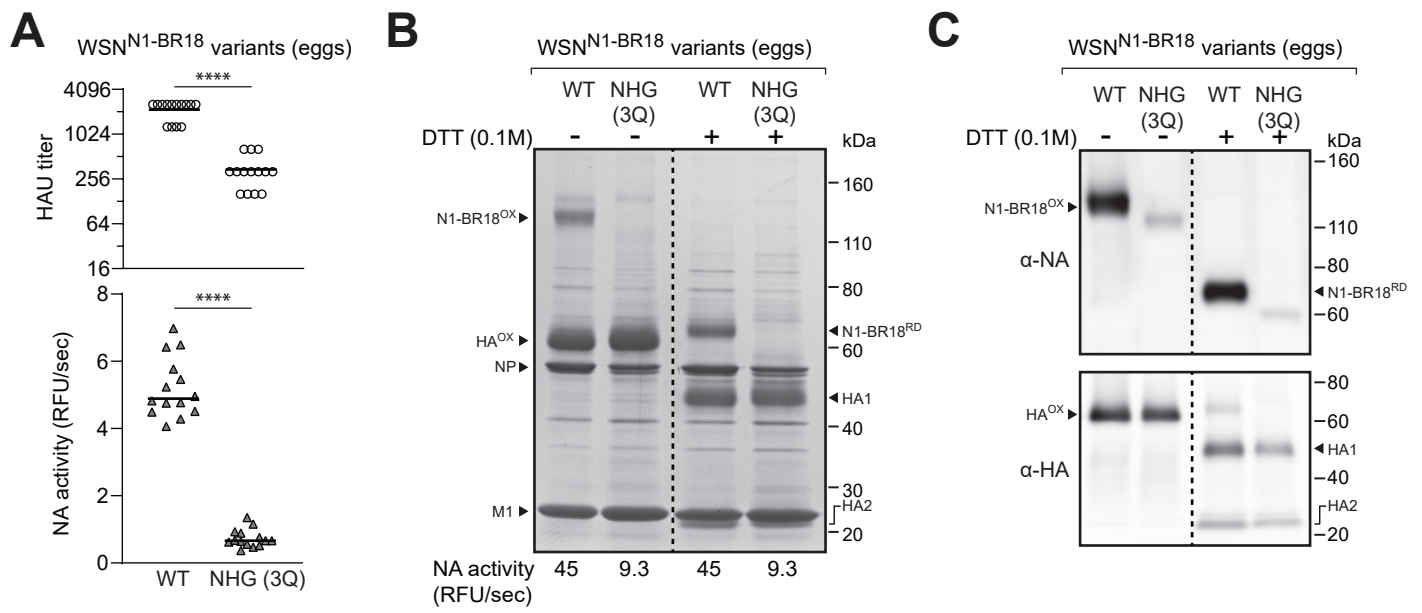


Figure 5

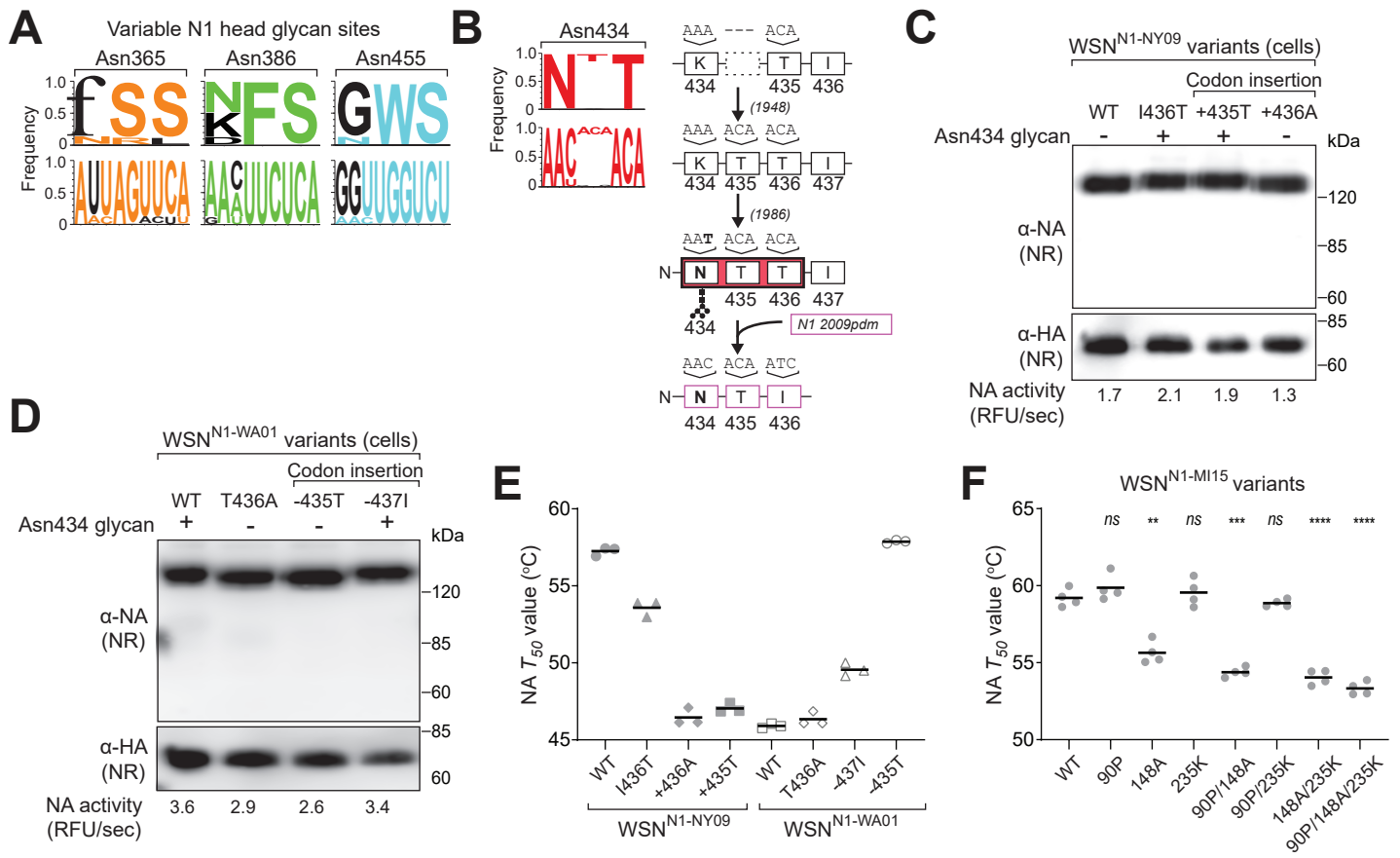


Figure 6

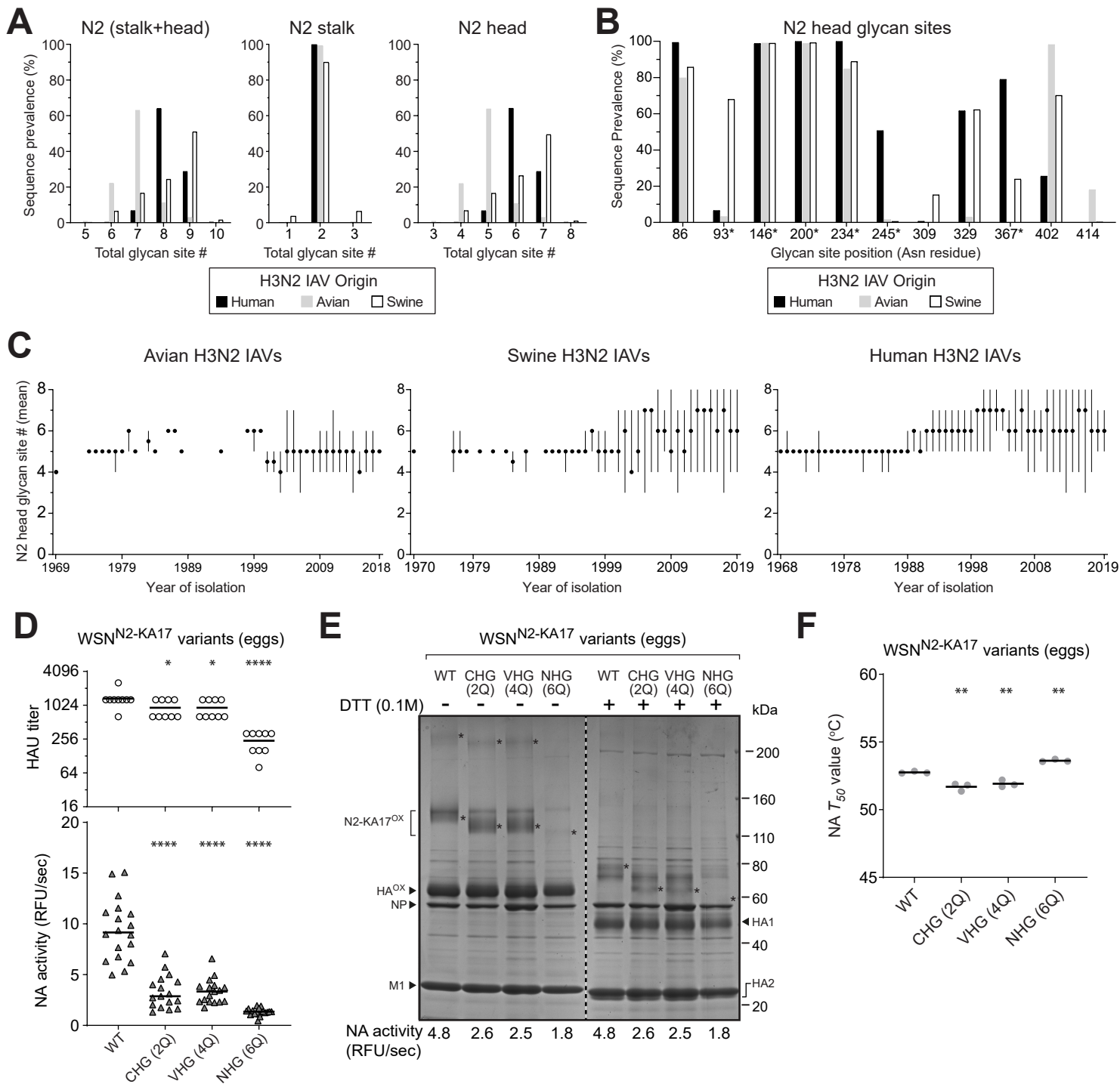


Figure 7